An MTL Theory Approach for the Simulation of MIMO Power Line Communication Channels

Fabio Versolatto, *Student Member, IEEE,* and Andrea M. Tonello, *Member, IEEE*

***Abstract*—We propose a bottom-up power line communication (PLC) channel simulator for networks that deploy multiconductor cables and allow establishing a multiple-input multiple-output (MIMO) communication link between two nodes. We show that the fundamental multiconductor transmission line (MTL) relations are a matrix form extension of the two-conductor transmission line equations, and that they allow the application of the voltage ratio approach (VRA) for the computation of the channel transfer function (CTF). Thus, any complex network can be remapped to obtain a simple representation in terms of MTL elementary units. Then, the MIMO CTF is computed as the product of the insertion loss of the units.**

We discuss the analytical computation of the per-unit-length (p.u.l.) parameters for two electrical cables, that we refer to as symmetric and ribbon. Further, we propose to use an improved cable model for ribbon cables that accounts for the dielectric non-uniformity. We report the comparison between simulation and experimental measures for two test networks. The results are in good agreement. This validates the proposed MIMO PLC channel simulation approach.

***Index Terms*—Power line communications, channel modeling, MIMO, multiconductor transmission lines.**

I. INTRODUCTION

POWER LINE communication systems are gaining high research and development interest because they can provide communication services by the exploitation of the large existent power line infrastructure both in outdoor and indoor scenarios. In particular, wide band state-of-the-art in-home PLC systems deliver high speed services via signal transmission over two conductors, i.e., the phase (hot) and the neutral wires, in the 1-30 MHz band [1]. To increase data rates beyond what it is offered today, larger bands should be used and/or advanced spectrally efficient transmission techniques should be developed.

Many power line networks deploy multiconductor cables. For safety reasons, in many countries the electrical regulations impose the use of a third conductor, typically referred to as protective earth (PE). The presence of a third conductor allows, in principle, establishing two parallel communication channels between the transmitter and the receiver. In general, with M conductors, $M-1$ communication channels are available between two nodes, which suggests the use of some form of multiple-input multiple-output communication. MIMO communications have attracted considerable attention in the wireless scenario, where multiple antennas are available. In this context, a great amount of research has been carried out to design spectral efficient modulation and coding techniques that are referred to as space-time and space-frequency coding techniques. Some early work on space-frequency coding algorithms for PLC has been reported in [2].

An important aspect is the characterization and modeling of PLC channels for the design and performance analysis of communication algorithms. Although several results about channel modeling for single-input single-output PLC channels are available, not many results are yet available for MIMO PLC channels. Deterministic bottom-up channel models for two-conductor PLC networks are described in [3] - [4]. They exploit transmission line (TL) theory under the transverse electromagnetic (TEM) or quasi TEM propagation assumption. They further require the knowledge of the topological information. Some work has also been done to provide a bottom-up statistical PLC channel model in [5]. More recently, a statistical model for in-home topologies combined with a bottom-up channel transfer function computation has allowed the realization of a statistically representative channel generator [6] - [7].

Besides the experimental MIMO channel characterization as it was done in [8] - [9], it is important to develop a model and a simulator for the CTF between two given nodes of a certain network taking into account for all the reflection and transmission effects that are due to line discontinuities. In [10], a bottom-up MIMO PLC channel simulator has been described. It is the MIMO extension of the two-conductor TL theory channel simulator presented in [4], which in turn exploits the method of the modal expression for the electrical quantities.

In this paper, we propose a bottom-up channel simulator that allows for the computation of the MIMO CTF for complex networks by exploiting the MTL theory concepts [11] under the TEM or quasi-TEM assumption. The method is inspired by the approach that we have presented in [3] for the two-conductor case. In detail, we show that the MTL relations of the method are a matrix form extension of the two-conductor TL equations. Furthermore, to simplify the problem, we propose to remap the network between the transmitter and receiver nodes in order to obtain a simple representation in terms of MTL elementary units. Then, the MIMO CTF is computed as the product of the insertion loss matrix of each MTL unit.

The analytical computation of the per-unit-length cable parameters, considering both a symmetric structure and a planar structure (ribbon cable), is also provided. To this end, we focus on three-conductor cables. We report both simulation and experimental measurements for two test networks, one without branches and one with a branch. We show that while

Manuscript received July 28, 2010; revised December 23, 2010; accepted February 16, 2011.

The authors are with the Dipartimento di Ingegneria Elettrica, Gestionale e Meccanica, DIEGM, Università di Udine, Udine 33100, Italy (e-mail: fabio.versolatto@uniud.it; tonello@uniud.it).

for the symmetric cable we obtain good agreement between the simulated and the measured results, with ribbon cables some more pronounced mismatches are found. Therefore, we propose to use an improved cable model that takes into account the non uniformity of the insulation material [12]. With this model, close matching between the simulation and experimental results is found.

The paper is organized as follows. In Section II, we summarize the MTL theory concepts and we derive the fundamental matrix form equations of the voltage ratio approach. In Section III, we address the cable models and we provide a comparison between the simulated and the experimental results. In Section IV, we discuss the effect of non-idealities and we improve the model taking into account the dielectric inhomogeneities. Finally, the conclusions follow.

II. Analysis of the MTL Configuration

We herein describe an MTL model for the simulation of MIMO in-home power line channels. We firstly report the fundamental MTL relations and we show that they are a matrix form extension of the two-conductor transmission line equations. Then, we propose an efficient method for the computation of the MIMO channel transfer function between pair of nodes in any complex power line network that deploys multiconductor cables. The method is based on a voltage ratio approach. For clarity, we first address the three-conductor case. Then, we consider the general multiconductor case.

A. Three-Conductor Transmission Line Equations

Several power line wiring installations use three identical wires, namely the phase, neutral and protective earth, that can be, in first approximation, modelled as parallel good conductors sheathed in a dielectric material and nearby placed. For instance, in Greece compact cables with conductors enclosed into a PVC cap are deployed [13]. In Italy, three conductors are individually insulated and placed inside small raceways. Some other countries deploy also ribbon cables.

In all cases, the transversal dimension of the overall cable structure is relatively small w.r.t. the transmission signal wavelength in the range of frequencies that we consider, i.e., in the lower GHz range. Therefore, we can make the TEM or quasi-TEM mode assumption [14], and we can adopt the per-unit-length parameter model also for non ideal cables [14].

In Fig. 1, we show a line section of three conductors of length Δx, where r_i, l_k, g_k, c_k with $i \in \{0, g, r\}$ and $k \in \{g, m, r\}$ denote the p.u.l. resistance, inductance, conductance and capacitance. The p.u.l. inductance l_m, capacitance c_m and conductance g_m take into account the mutual interactions between conductors. The bottom conductor is assumed to be the neutral, while the middle and the upper most conductors are respectively, the PE and the phase. We assume the neutral to be the reference conductor, and the phase and PE currents to return through the neutral conductor. Consequently, two different circuits sharing the same return conductor can be defined. Coupling effects provide interactions between them, therefore by transmitting and receiving on both the circuits, a 2×2 MIMO system is defined. The first circuit comprises

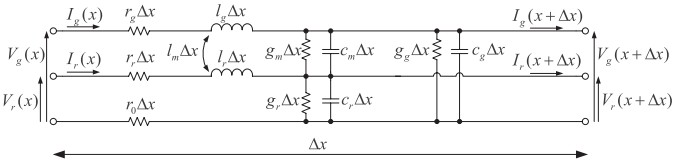

Fig. 1. Per-unit-length equivalent model of the three conductor line.

the phase and the neutral wires. We refer to it as generator circuit. The second circuit comprises the PE and the neutral wires. We refer to it as receptor circuit.

Now, in order to provide a steady-state analysis, we use the phasor representation for electrical quantities. We denote with $V_k(f, x)$, for $k \in \{g, r\}$, the voltage phasors associated to the generator circuit and the receptor circuit at frequency f and coordinate x. Thus, the voltage in sinusoidal regime is $v_k(x,t) = \mathrm{Re}\{V_k(x,f)e^{j2\pi ft}\}$. To simplify the notation, we do not explicitly show the frequency dependency in the following. Therefore, we simply write $V_k(x)$. By letting $\Delta x \to 0$ in Fig. 1, we obtain the telegraph equations in the frequency domain, that read as follows

$$\frac{\partial \mathbf{V}(x)}{\partial x} = -\big(\mathbf{R} + j2\pi f\mathbf{L}\big)\mathbf{I}(x)\,, \tag{1}$$

$$\frac{\partial \mathbf{I}(x)}{\partial x} = -\big(\mathbf{G} + j2\pi f\mathbf{C}\big)\mathbf{V}(x)\,, \tag{2}$$

where $\mathbf{V} = [V_g,\ V_r]^T$ is the voltage phasor vector, $\mathbf{I} = [I_g,\ I_r]^T$ is the current phasor vector and $\{\cdot\}^T$ denotes the transposition. Furthermore,

$$\mathbf{R} = \begin{bmatrix} r_g + r_0 & r_0 \\ r_0 & r_r + r_0 \end{bmatrix}, \quad \mathbf{L} = \begin{bmatrix} l_g & l_m \\ l_m & l_r \end{bmatrix},$$

$$\mathbf{C} = \begin{bmatrix} c_g + c_m & -c_m \\ -c_m & c_r + c_m \end{bmatrix}, \quad \mathbf{G} = \begin{bmatrix} g_g + g_m & -g_m \\ -g_m & g_r + g_m \end{bmatrix},$$

are the p.u.l. parameter matrices for the resistance, inductance, capacitance and conductance, respectively.

Now, if we define the impedance and the admittance matrix as $\mathbf{Z} = \mathbf{R} + j2\pi f\mathbf{L}$ and $\mathbf{Y} = \mathbf{G} + j2\pi f\mathbf{C}$, respectively, by means of a first derivative and a substitution we obtain the MTL equations

$$\frac{\partial^2 \mathbf{V}(x)}{\partial x^2} = \mathbf{ZY}\,\mathbf{V}(x)\,, \tag{3}$$

$$\frac{\partial^2 \mathbf{I}(x)}{\partial x^2} = \mathbf{YZ}\,\mathbf{I}(x)\,, \tag{4}$$

that are coupled by the boundary line conditions, and thus we can focus only on a single one. Considering (4), we can use the eigenvalue decomposition to obtain

$$\mathbf{YZ} = \mathbf{T}\begin{bmatrix} \lambda_1 & 0 \\ 0 & \lambda_2 \end{bmatrix}\mathbf{T}^{-1} = \mathbf{T}\mathbf{\Lambda}\mathbf{T}^{-1}\,, \tag{5}$$

where $\mathbf{T}$ and $\mathbf{\Lambda}$ are the eigenvector and eigenvalue matrices of $\mathbf{YZ}$, respectively. Then, we diagonalize (4) defining the modal current vector $\mathbf{I}_m = \mathbf{T}^{-1}\mathbf{I}$ such that

$$\frac{\partial^2 \mathbf{I}_m(x)}{\partial x^2} = \mathbf{\Lambda}\mathbf{I}_m(x)\,. \tag{6}$$

Now, due to the diagonal nature of $\mathbf{\Lambda}$, the resultant system comprises two uncoupled equations that can be independently solved leading to

$$\mathbf{I}_m(x) = \begin{bmatrix} e^{-\gamma_1 x} & 0 \\ 0 & e^{-\gamma_2 x} \end{bmatrix} \mathbf{I}_m^+ + \begin{bmatrix} e^{\gamma_1 x} & 0 \\ 0 & e^{\gamma_2 x} \end{bmatrix} \mathbf{I}_m^- , \quad (7)$$

where $\mathbf{I}_m^+$ and $\mathbf{I}_m^-$ are vectors whose coefficients are determined from the boundary conditions, and γ_1, γ_2 are the propagation constants obtained from the diagonal elements of $\mathbf{\Lambda}$. In detail, we define the propagation constant matrix $\mathbf{\Gamma} = diag\{\gamma_1, \gamma_2\}$, as the one for which $\mathbf{\Gamma\Gamma} = \mathbf{\Lambda}$. Finally, we exploit the relation $\mathbf{I} = \mathbf{T}\mathbf{I}_m$ to obtain the expression for the current phasor vector $\mathbf{I}$ and the voltage vector $\mathbf{V}$ that read

$$\mathbf{I}(x) = \mathbf{T}\mathbf{I}_m = \mathbf{T}\left(\mathbf{e}^{-\mathbf{\Gamma}x}\mathbf{I}_m^+ + \mathbf{e}^{\mathbf{\Gamma}x}\mathbf{I}_m^-\right), \quad (8)$$

$$\mathbf{V}(x) = \mathbf{Y}^{-1}\mathbf{T}\mathbf{\Gamma}\left(\mathbf{e}^{-\mathbf{\Gamma}x}\mathbf{I}_m^+ - \mathbf{e}^{\mathbf{\Gamma}x}\mathbf{I}_m^-\right), \quad (9)$$

respectively. The voltages and the currents maintain the same structure of the two-conductor line case, i.e., both are expressed as the superposition of the transmitted and reflected waves.

To proceed, we firstly define the characteristic impedance matrix of the multiconductor transmission line as $\mathbf{Z}_C = \mathbf{Y}^{-1}\mathbf{T}\mathbf{\Gamma}\mathbf{T}^{-1}$. Then, we define the load reflection coefficient matrix as the matrix $\boldsymbol{\rho}_{L_I}$ such that $\mathbf{I}_m^- = \boldsymbol{\rho}_{L_I}\mathbf{I}_m^+$, where the subscript $\{\cdot\}_I$ is used in the notation to recall that we are dealing with currents. Finally, from (8)-(9), it follows that

$$\mathbf{I}(0) = \mathbf{T}(\mathbf{U} + \boldsymbol{\rho}_{L_I})\mathbf{I}_m^+ , \quad (10)$$

$$\mathbf{V}(0) = \mathbf{Z}_C\mathbf{T}(\mathbf{U} - \boldsymbol{\rho}_{L_I})\mathbf{I}_m^+ , \quad (11)$$

where $\mathbf{U}$ is the identity matrix of size 2×2, and we assume that the load is placed at the coordinate $x = 0$.

Now, we define the load admittance matrix $\mathbf{Y}_L$ as the matrix such that $\mathbf{I}(0) = \mathbf{Y}_L\mathbf{V}(0)$, and thus we rewrite the reflection coefficient matrix as

$$\boldsymbol{\rho}_{L_I} = \mathbf{T}^{-1}\mathbf{Y}_C\big(\mathbf{Y}_L + \mathbf{Y}_C\big)^{-1}\big(\mathbf{Y}_L - \mathbf{Y}_C\big)\mathbf{Z}_C\mathbf{T} , \quad (12)$$

where $\mathbf{Y}_C = \mathbf{Z}_C^{-1}$. Furthermore, once $\mathbf{Y}_L$ is known, we can also determine the admittance matrix $\mathbf{Y}_R(x)$ at coordinate x as the matrix that satisfies the relation $\mathbf{I}(x) = \mathbf{Y}_R(x)\mathbf{V}(x)$. $\mathbf{Y}_R(x)$ can be interpreted as the load admittance carried back at coordinate x. Combining (8)-(9), it follows that

$$\mathbf{Y}_R(x) = \mathbf{T}\big(\mathbf{e}^{-\mathbf{\Gamma}x} + \mathbf{e}^{\mathbf{\Gamma}x}\boldsymbol{\rho}_{L_I}\big) \times \big(\mathbf{e}^{-\mathbf{\Gamma}x} - \mathbf{e}^{\mathbf{\Gamma}x}\boldsymbol{\rho}_{L_I}\big)^{-1}\mathbf{T}^{-1}\mathbf{Y_C} . \quad (13)$$

This final relation will be exploited in the next section for the development of a CTF simulator for complex in-home networks that comprise several branches and loads.

B. Voltage Ratio Approach for Three-Conductor Networks

Our objective is to compute the MIMO channel transfer function of any pair of nodes in power line networks that comprise multiconductor lines and several branches and loads. We propose to compute the CTF via an MTL extension of the algorithm presented in [3] for the two-conductor case. We firstly remap the MTL network into a backbone and into a set of branches that depart from intermediate nodes of the backbone. The backbone is the shortest signal path between the transmitter and the receiver. Fig. 2 shows an example of a remapped network where each backbone branch comprises sub-branches and loads at the terminal nodes.

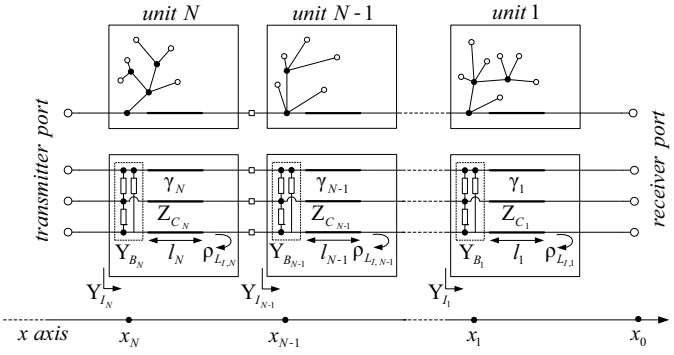

Fig. 2. On top, unifilar description of a topology remapped in units. On bottom, equivalent representation of the units in admittance matrix terms.

We can model the whole branch (single or multi level) that departs from the backbone node n_b as an equivalent admittance directly connected to n_b. Strictly, the equivalent admittance matrix $\mathbf{Y}_{B_b}$ is obtained by carrying back the terminal loads (comprising open loads) up to the backbone node. To this aim, we recursively apply (13). The final result is a simple representation of the network seen by a pair of nodes, namely, an MTL backbone with a number of admittances in certain points.

To proceed, we split the backbone into N small elements called units. In Fig. 2, we show an example of unit representation of the network. We use thick and thin lines to represent physical wires and zero-length connections, respectively. The coordinates on the x axis refer to the position of the backbone nodes. Each unit $b = 1, \ldots, N$ contains an homogeneous piece of backbone line and the equivalent admittance of the branch connected to the node n_b. We conventionally start the unit numeration from the receiver end. We also denote with $\mathbf{Z}_{C_b}$, $\mathbf{\Gamma}_b$, l_b and $\boldsymbol{\rho}_{L_{I,b}}$, the characteristic impedance matrix, the propagation constant matrix, the length of the piece of backbone line, and the load reflection matrix of the unit b, respectively. The latter is given by (12). Further, we refer to $\mathbf{Y}_{L_b}$ and $\mathbf{Y}_{I_b}$ as the load and the input admittance matrices of the unit b, respectively. The first is the receiver admittance matrix when $b = 1$, otherwise it is the input admittance matrix of the unit $b - 1$. The latter is the sum of the load admittance matrix $\mathbf{Y}_{L_b}$ carried back at the input port of the unit b, and the branch admittance matrix $\mathbf{Y}_{B_b}$.

Now, from (9) and (11), the voltage vector at node n_b can be written as a function of the voltage vector at node n_{b-1} yielding

$$\mathbf{V}(x_b) = \mathbf{Z}_{C_b}\mathbf{T}_b\big(\mathbf{e}^{\mathbf{\Gamma}_b l_b} - \mathbf{e}^{-\mathbf{\Gamma}_b l_b}\boldsymbol{\rho}_{L_I,b}\big) \times \big(\mathbf{U} - \boldsymbol{\rho}_{L_I,b}\big)^{-1}\mathbf{T}_b^{-1}\mathbf{Z}_{C_b}^{-1}\mathbf{V}(x_{b-1}) . \quad (14)$$

By definition, the MTL CTF of a given unit is the voltage

insertion loss between the two ports of the unit, namely,

$$\mathbf{V}(x_{b-1}) = \mathbf{H}_b \mathbf{V}(x_b)\,. \tag{15}$$

Thus, from (14) it follows that

$$\mathbf{H}_b = \mathbf{Z}_{C_b}\mathbf{T}_b\big(\mathbf{U} - \boldsymbol{\rho}_{L_I,b}\big) \times \left(\mathbf{e}^{\boldsymbol{\Gamma}_b l_b} - \mathbf{e}^{-\boldsymbol{\Gamma}_b l_b}\boldsymbol{\rho}_{L_i,b}\right)^{-1}\mathbf{T}_b^{-1}\mathbf{Z}_{C_b}^{-1}\,. \tag{16}$$

Now, we define the voltage phasor vectors at the transmitter and receiver nodes as $\mathbf{V}(x_N, f)$ and $\mathbf{V}(x_0, f)$, respectively. We explicitly show the frequency dependency of the quantities. Hence, if we denote with $\mathbf{H}(f)$ the overall MTL transfer function (insertion loss), we obtain $\mathbf{V}(x_0, f) = \mathbf{H}(f)\mathbf{V}(x_N, f)$. Finally, by recursively applying (15), the CTF can be computed as follows

$$\mathbf{H}(f) = \prod_{b=1}^{N} \mathbf{H}_b(f)\,, \tag{17}$$

i.e., the product of the CTF of the units. We refer to this method as MTL voltage ratio approach.

C. Application of the VRA and Complexity Analysis

In order to detail the application of the VRA, we firstly apply it to the branched test network shown in Fig. 3(b). We start dividing the network in units. According to the notation of Fig. 2, two units exist. The first includes the line of length l_3 and the branch terminated into $\mathbf{Y}^{br}$. The second unit comprises the piece of backbone line of length l_1. For the first unit, we have to calculate the insertion loss and the input admittance matrix. To this end, we compute twice the relations (12)-(13), once the relation (16), and then, at the input port of the unit, we sum the equivalent admittance matrices of the branch and the receiver. The second unit is rather simple since no branches are present, and thus we only need to compute (12) and (16) once. Finally, the overall CTF is given by (17).

Now, if we consider a more complex network, we can still divide it into units, and then, for each unit, we compute the same relations applied before to the branched test network. Therefore, the number of relations to be solved by the VRA scales linearly with the total number of network units.

For the sake of comparison, we can consider the method proposed in [10], which is in general more complex because it does not consider the division of the network in units as we instead propose. However, it can be also applied once the network is divided into units. In such a case, the number of relations to be solved for a given unit is similar in method [10] and in our method. However, the computation of the relations requires a higher number of scalar operations (additions and products) per unit in the method [10] compared to the VRA. As an example, for the network of Fig. 3(b) the method in [10] runs approximately 3% more operations than the VRA. It follows, that also for more complex networks the VRA maintains some complexity advantage.

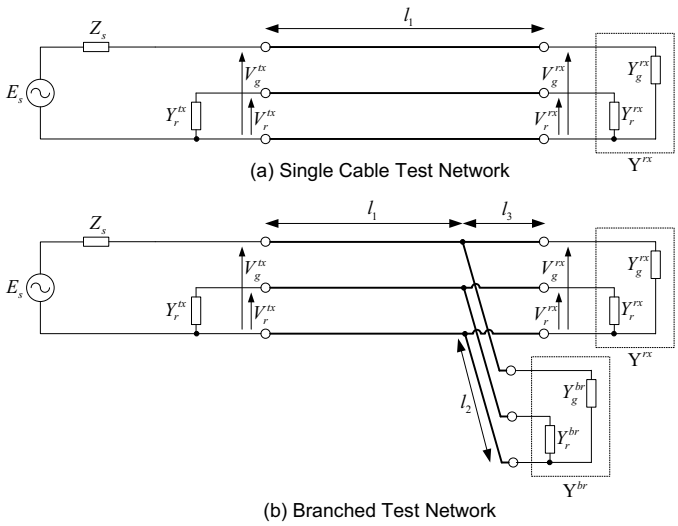

Fig. 3. Equivalent representation of the two test networks.

D. Multiconductor Extension of the VRA

Although the three-conductor case is the most frequent in in-home PLC networks, the VRA can be easily extended when $M > 3$ conductors are present, e.g., in multiple phase networks. In this case, $M - 1$ communication channels are available. By knowing the p.u.l. parameters of the cables, we derive the relations (3)-(4) of size $M-1$. Then, we diagonalize the system of equations through the eigenvalue decomposition so that the results of Section II-A are still valid, and the VRA of Section II-B is applicable.

III. Validation of the Model

In this section we report experimental results in order to validate the analytical approach that we have proposed. We consider two test networks that are depicted in Fig. 3. In the first network, we consider the transmitter and the receiver directly connected via a three-conductor homogeneous piece of line, i.e. the backbone. In the second network, we evaluate the effect of a branch connected to the backbone. We refer to the two networks as single section and branched, respectively. The cable geometries of Fig. 4 are considered, i.e., a symmetric cable and a planar (ribbon) cable. The geometrical and electrical properties of the cables are summarized in Table I, while the lengths of the MTL lines are reported in Table II. We terminate the branch into a load whose admittance matrix reads

$$\mathbf{Y}^{br} = \begin{bmatrix} Y_g^{br} & 0 \\ 0 & Y_r^{br} \end{bmatrix} = \begin{bmatrix} 1/50 & 0 \\ 0 & 0 \end{bmatrix}\,. \tag{18}$$

The measurements have been made in the time domain using a signal pulser and a two channels digital oscilloscope with $50\ \Omega$ input impedance. This realizes a form of single-input multiple-output (SIMO) transmission since the transmitter (signal pulser) is connected to a pair of conductors, e.g., the phase and neutral, while the receiver captures both the signals between the phase and neutral, and between the PE and neutral. The frequency response, up to 80 MHz, has been

TABLE I
PARAMETERS OF THE CABLES

Type	r_w / r_d / d (mm)	n_s / n_e	σ_c / σ_d (S/m)
Symm.	0.69 / 1.5 / 3.1	16/6	$5.8 \cdot 10^7 / 10^{-5}$
Ribbon	0.79 / 1.6 / 3.4	15 / 13	

TABLE II
CIRCUIT CABLE LENGTHS

l_1 (m)	l_2 (m)	l_3 (m)
5.22	2.30	3.60

obtained via discrete Fourier transform with a frequency step size of $50\,kHz$.

We model the receiver as a quadripole with a shared reference conductor and two admittances connected at the end of the receptor and generator circuits, respectively. Thus, the admittance matrix of the receiver can be written as $\mathbf{Y}^{rx} = diag\{Y_g^{rx}, Y_r^{rx}\}$, where we conventionally set $Y_g^{rx} = Y_r^{rx} = 1/50\,S$. We also terminate the receptor circuit at the transmitter side into $Y_r^{tx} = 1/50\,S$. It follows that both ends of the receptor circuit are connected to an admittance of the same value.

We define the "direct" insertion loss $H_d(f)$ as the ratio $V_g^{rx}(f)/V_g^{tx}(f)$, and the "coupled" insertion loss $H_c(f)$ as the ratio $V_r^{rx}(f)/V_g^{tx}(f)$. Then, the SIMO insertion loss vector is

$$\mathbf{H}_{\text{SIMO}}(f) = \begin{bmatrix} H_d(f) \\ H_c(f) \end{bmatrix} = \begin{bmatrix} V_g^{rx}(f)/V_g^{tx}(f) \\ V_r^{rx}(f)/V_g^{tx}(f) \end{bmatrix}. \tag{19}$$

Now, we refer to

$$\mathbf{Y}_{I_N}(f) = \begin{bmatrix} Y_{I_{11}}(f) & Y_{I_{12}}(f) \\ Y_{I_{21}}(f) & Y_{I_{22}}(f) \end{bmatrix} \tag{20}$$

as the input line admittance matrix at the transmitter side. According to the notation of Fig. 3, it follows that

$$\begin{bmatrix} I_g^{tx}(f) \\ I_r^{tx}(f) \end{bmatrix} = \mathbf{Y}_{I_N}(f) \begin{bmatrix} V_g^{tx}(f) \\ V_r^{tx}(f) \end{bmatrix}. \tag{21}$$

Furthermore, the current and the voltage at the transmitter side of the receptor circuit are related as follows, $I_r^{tx}(f) = -Y_r^{tx} V_r^{tx}(f)$. Therefore, from (21) we obtain

$$V_r^{tx}(f) = -\frac{Y_{I_{21}}(f)}{Y_{I_{22}}(f) + Y_r^{tx}} V_g^{tx}(f) \tag{22}$$

Finally, from (17) and (22) we can reformulate $\mathbf{H}_{\text{SIMO}}(f)$ as

$$\mathbf{H}_{\text{SIMO}}(f) = \mathbf{H}(f)\boldsymbol{\alpha}(f)\,, \tag{23}$$

where $\boldsymbol{\alpha}(f) = \left[1 \;\; -Y_{I_{21}}(f)/(Y_{I_{22}}(f) + Y_r^{tx})\right]^T$ takes into account for the boundary condition at the transmitter side of the receptor circuit.

In the following, we firstly discuss how to obtain the p.u.l. parameters for the cable geometries herein considered. Then, we compare the simulations with the experimental results.

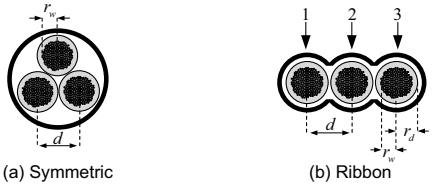

(a) Symmetric (b) Ribbon

Fig. 4. Cross sections of the two considered cables.

A. P.u.l. Parameters for the Symmetric Cable

The computation of the p.u.l. parameter matrices $\mathbf{R}$, $\mathbf{L}$, $\mathbf{C}$ and $\mathbf{G}$ can be done in an analytical way for the symmetric cable geometry shown in Fig. 4(a). We further assume the general case of stranded conductors that are independently sheathed and then enclosed into a second PVC cap. The inter-distance between the conductors is constant. We also approximate the dielectric as homogeneous since the three-conductor structure is typically compact.

To determine the p.u.l. resistance of a stranded conductor, we follow the approach in [15], where the resistance of a solid core conductor is divided by a correction coefficient X_R, i.e., $r = r_{\text{solid}}/X_R$ with

$$r_{\text{solid}} = \begin{cases} 1/(\sigma_c \pi r_w^2) & \delta >> r_w\,, \\ \sqrt{\mu_0 f/(4\sigma_c \pi r_w^2)} & \delta << r_w\,, \end{cases} \tag{24}$$

where r_w is the radius of the solid core conductor, σ_c is the conductivity, $\delta = 1/\sqrt{\pi \mu_0 f \sigma_c}$ [14] is the skin depth with f being the frequency and μ_0 being the vacuum permeability.

Therefore, X_R is the ratio between the areas interested by the flow of the current in the stranded wire and in the solid core conductor. Further, the current is supposed to flow only in the n_e outermost conductors of the stranded wires. Thus, it follows that [15]

$$X_R = n_e \frac{\cos^{-1}(\frac{r_s - \delta}{r_s}) r_s^2 - (r_s - \delta)\sqrt{r_s^2 - (r_s - \delta)^2}}{2 r_w \delta}\,, \tag{25}$$

where n_e and r_s denote the number of strand wires that constitutes the outer ring and their radius, respectively. In particular, we compute r_s as $r_s \simeq r_w/\sqrt{n_s}$ where n_s denotes the total number of strands that make up the conductor core. The correction factor is derived assuming that the solid-core conductor has a non perfectly circular cross section (corrugated circle) due to the outer ring of thin wires. We point out that in [11] another approach is followed. It consists in dividing the p.u.l. resistance of a solid wire by the number of strands. However, we have found through measurements that the approach in [15] performs better.

Assuming that the phase, neutral and ground wires have the same geometrical and electrical properties, we have that $r_g = r_r = r_0 = r$. Conversely, $\mathbf{L}$, $\mathbf{C}$ and $\mathbf{G}$ depend in general on the overall geometry of the cable, i.e. the distance between conductors. However, under the assumption of an homogeneous dielectric, the p.u.l. parameter matrices fulfill the following relations [14]

$$\mathbf{LC} = \mu_0 \varepsilon_0 \varepsilon_r \mathbf{U} \tag{26}$$

$$\mathbf{LG} = \mu_0 \sigma_d \mathbf{U} \tag{27}$$

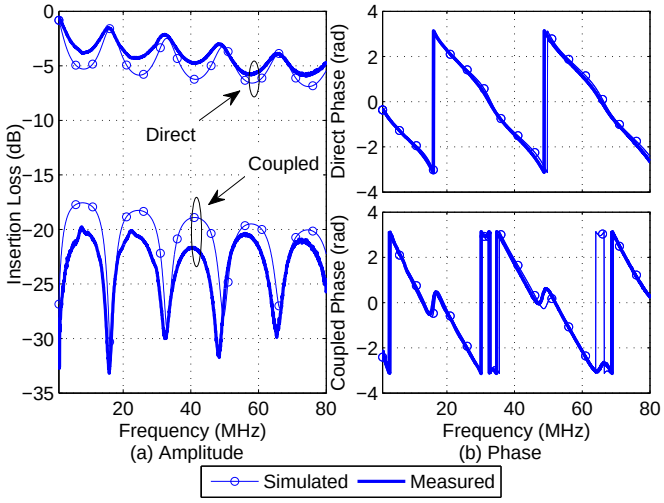

Fig. 5. Comparison between the simulated (circle-marked line) and measured (solid line) results of the direct and coupled insertion losses of the single section test network. (a) amplitudes, and (b) phases.

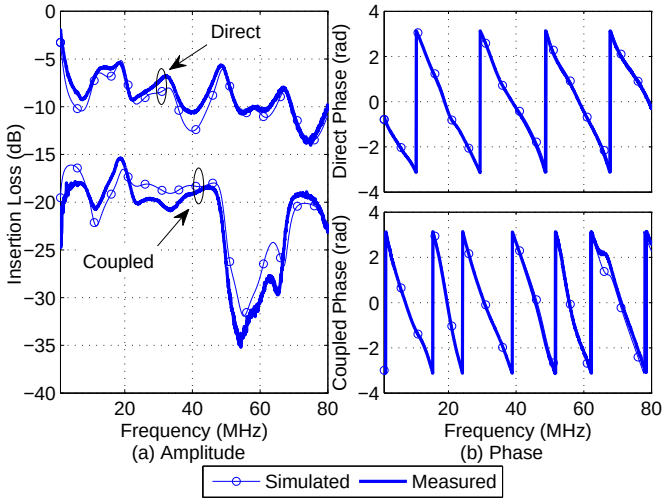

Fig. 6. Comparison between the simulated (circle-marked line) and measured (solid line) results of the direct and coupled insertion losses of the branched test network. (a) amplitudes, and (b) phases.

where ε_0, ε_r and σ_d are respectively the vacuum dielectric constant, the relative dielectric constant, and the conductivity of the dielectric among conductors, while $\mathbf{U}$ is the 2×2 identity matrix. Thus, for each cable we only need to compute the p.u.l. inductance matrix, since the $\mathbf{C}$, $\mathbf{G}$ matrices are consequently defined from (26)-(27). Due to the nature of the structure and according to the notation of Fig. 4, it is immediate to verify that

$$l_g = l_r = 2l_m = \frac{\mu_0}{\pi} \log\left(\frac{d}{r_w}\right),$$

where l_m takes only into account for the external inductance, i.e., it neglects the internal inductance of a non-null section cable [14].

To compare the simulation results with the experimental ones, we have used the electrical constants presented in Table I. The frequency-dependent dielectric constant can be obtained from the measurement of the speed of light $v(f)$ as $\varepsilon_r(f) = 1/(\varepsilon_0 \mu_0 v(f)^2)$. Via measurements, we have found that $\varepsilon_r(f)$ can be approximated as

$$\varepsilon_r(f) = \frac{1.6661 \cdot 10^{-6}}{f} + 2.9701\,. \tag{28}$$

B. Comparison between Simulations and Measurements for the Symmetric Cable

In the following, the amplitude and phase of the channel transfer functions are defined as $A_k(f) = 20\log_{10}(|H_k(f)|)$ and $\varphi_k(f) = \angle H_k(f)$, respectively, where $k \in \{d, c\}$ denotes the direct and coupled channel in a SIMO configuration. When symmetric cables are used in the single section test network, the p.u.l. parameters are the same for the generator and the receptor circuit. Thus, identical results are found whether we transmit between the phase and neutral conductor or between the PE and neutral conductor.

In Fig. 5, we compare the simulated results with the experimental ones for the single section test network. The comparison is made in terms of both the direct and the coupled amplitude and phase of the CTF. The results are in excellent agreement especially for the direct CTF. In particular, the phase is perfectly matching. The relatively small discrepancy in the amplitude (always below 3 dB) is due to the non idealities that are neglected by the simulations.

In Fig. 6, we show the results for the branched test network. Again, the results are in good agreement both for the direct and the coupled channels, which proves the validity of the proposed simulation method.

C. P.u.l. Parameters for the Ribbon Cable and Experimental Validation

The definition of the reference conductor in the ribbon cables is important in order to determine the p.u.l. parameters. In particular, referring to the notation of Fig. 4(b), if the wire labelled with 2 is the reference conductor, then we can compute the p.u.l. inductances as [14]

$$l_g(2) = l_r(2) = \frac{\mu_0}{\pi} \log\left(\frac{d}{r_w}\right), \quad l_m(2) = \frac{\mu_0}{2\pi} \log\left(\frac{d}{2r_w}\right),$$

where in the notation we highlight the dependence of each inductance on the reference conductor.

If the reference conductor is an external wire, namely 1 or 3, the generator and receptor circuits are not equivalent. Thus, we define the generator circuit between the two external wires, and the receptor circuit consequently. The p.u.l. inductances for this case read [11]

$$l_g(1) = l_g(3) = 2l_m(1) = 2l_m(3) = \frac{\mu_0}{\pi} \log\left(\frac{2d}{r_w}\right),$$
$$l_r(1) = l_r(3) = \frac{\mu_0}{\pi} \log\left(\frac{d}{r_w}\right).$$

Note that the p.u.l. inductances do not depend on the dielectric permeability. Hence, they are not affected by insulation inhomogeneities and the previous relations are valid in general.

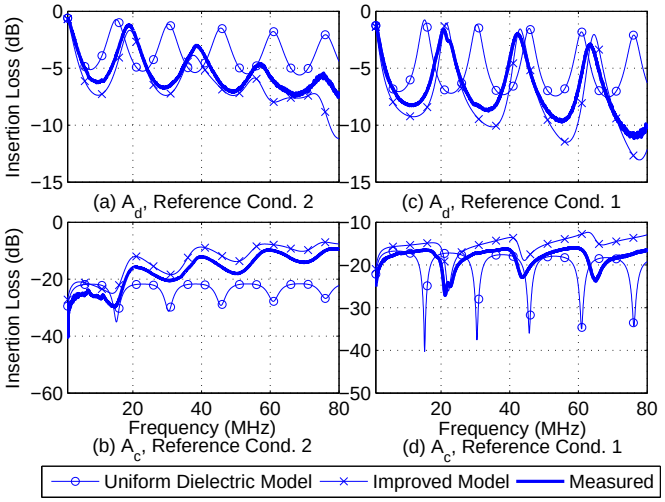

Fig. 7. Comparison between the simulated and measured results of the direct and coupled insertion losses for the single section test network when a ribbon cable is deployed. Results are obtained considering the central reference conductor in (a)-(b), and an external reference conductor in (c)-(d).

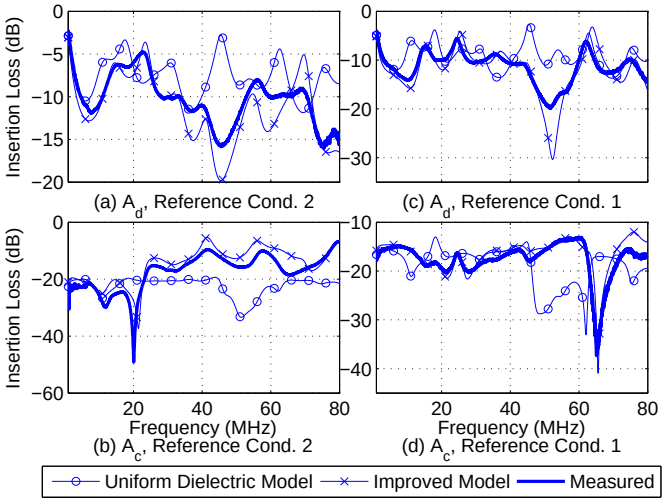

Fig. 8. Comparison between the simulated and measured results of the direct and coupled insertion losses for the branched test network when a ribbon cable is deployed. Results are obtained considering the central reference conductor in (a)-(b), and an external reference conductor in (c)-(d).

Now, if we neglect the dielectric inhomogeneities, we can still exploit (26)-(27) in order to obtain the $\mathbf{C}$ and $\mathbf{G}$ matrices.

In Fig. 7, we report the comparison between simulation and experimental results for the single section test network that uses the ribbon cable. The geometrical parameters of the ribbon cable are reported in Table I. Further, for the ribbon cable we have found an almost frequency independent relative dielectric constant, i.e., $\varepsilon_r = 3.5$. Both reference conductor configurations are considered. Namely, the central conductor case and an external conductor case are shown in Fig. 7(a)-7(b) and Fig. 7(c)-7(d) respectively. We report only the amplitude of the CTF. The solid curves are the measured results, while the curves with circle markers are those obtained via simulation under the assumption of a uniform dielectric. Discrepancies are found both for the direct and the coupled channels, i.e., the simulated insertion losses are not perfectly consistent with the measures. This effect is more pronounced when the reference is the central conductor rather than an external one.

In Fig. 8, we show the same results for the branched test network described in Section III. Also in this case discrepancies are found.

In the next section, we further investigate the reasons of such discrepancies, and we propose an improved cable model based on a finer characterization of the dielectric inhomogeneities.

IV. Model Improvements and Validation

In the previous section, we have found close matching between the simulated and measured channel transfer functions when the symmetric cable is deployed. Slight differences are due to the presence of non idealities of a real-made circuit. In fact, the theoretical model applies some approximations, i.e., we model the line geometry as constant, we consider the dielectric around conductors as uniform, we do not take into account the fact that the hand-made wiring interconnections are not ideal as those at the branch nodes and between the test network and the measurement equipment ports. Nevertheless, these approximations have yielded good matching of the results when the symmetric cable is used. On the contrary, with the ribbon cable the discrepancy is significant, as Fig. 7 and Fig. 8 show, still considering an identical test network topology. This suggests that the conventional ribbon cable model does not represent with sufficient accuracy the reality. Therefore, we have further refined the ribbon cable model as follows.

From Fig. 4(b), we note that the conductors of a ribbon cable are surrounded only by a thin insulation layer. Therefore, the conventional assumption of a uniform dielectric may strongly affect the mutual interactions between coupled channels. The problem has been already pointed out in the literature, where a refined characterization of the charge densities is proposed in [12]. In detail, the charge over each conductor surface is no longer determined by just the position of the other wires. It is also affected by the presence of a bound charge over the dielectric discontinuity surfaces. In particular, the charge distribution over the conductors is the sum of the free charge and the bound charge. The bound charge over the conductor surface is equal in absolute value and opposite in sign to the bound charge q_b over the dielectric surface, i.e., the discontinuity dielectric surface. According to [12], if we accurately model the bound charge q_b, we are able to estimate the free charge q_f on each conductor surface and consequently we obtain an improved model for the capacitance matrix $\mathbf{C}$.

To this end, we follow the approach proposed in [12]. The method describes the surface charge densities over the discontinuity surfaces with a Fourier series expansion. Then, two sets of boundary conditions are enforced. The first defines the potential over each conductor as a function of the charge densities. The second imposes the continuity conditions for the normal components of the displacement vector just inside and just outside the dielectric surfaces. The resultant system of equations leads to an expression of the charge densities

as a function of the conductor potentials, and thus to the the free charge over the conductors. Finally, by defining the conductor potentials as a function of the reference potential, the p.u.l. capacitance matrix $\mathbf{C}$ is obtained. This is done for both transmission configurations, i.e., when the reference conductor is the wire 2 or one of the external wires. Finally, once $\mathbf{C}$ is known, we apply (26)-(27) to derive the inductance matrix $\mathbf{L}$ and the conductance matrix $\mathbf{G}$.

We report numerical results in Fig. 7 and 8, where the cross-marked curves represent the insertion loss computed with the improved ribbon cable model. Now, a significant better matching between simulated and measured results is shown for both the single section and the branched test network. For instance, in Fig. 7(b) (single section network) and 8(d) (branched network), the simulated insertion loss for the coupled channel is always within 4 dB from the measured one, while the simulated results with the conventional cable model are significantly discrepant.

V. CONCLUSIONS

We have presented an MTL theory based approach to compute the MIMO channel transfer function of PLC networks with multiple conductor cables. The method is based on computing the MIMO CTF via a matrix voltage ratio approach which is applicable to complex in-home networks that exhibit several branches. We have addressed the analytical modelling of cables with symmetric and ribbon geometries. Then, we have validated the channel simulator. We have found that the results from simulations are in good agreement with the experimental ones. This shows that the simulator is an appropriate tool for the generation of MIMO PLC channel responses to be used in the design and testing of PLC modems that exploit MIMO signal processing. In order to better the results when ribbon cables are deployed, we have also proposed to improve the cable model by considering the effects of a non uniform dielectric insulation.

REFERENCES

[1] S. Galli and O. Loginov, "Recent Developments in the Standardization of Power Line Communications within the IEEE," *IEEE Commun. Mag.*, vol. 46, no. 7, pp. 64–71, Jul. 2008.

[2] C. L. Giovaneli, B. Honary, and P. G. Farrell, "Space-Frequency Coded OFDM System for Multi-Wire Power Line Communications," in *Proc. IEEE Int. Symp. Power Line Commun. and its App. (ISPLC)*, Apr. 2005, pp. 191–195.

[3] A. M. Tonello and T. Zheng, "Bottom-Up Transfer Function Generator for Broadband PLC Statistical Channel Modeling," in *Proc. IEEE Int. Symp. Power Line Commun. and its App. (ISPLC)*, Apr. 2009, pp. 7–12.

[4] J. Anatory, N. Theethayi, and R. Thottappillil, "Power-Line Communication Channel Model for Interconnected Networks - Part I: Two-Conductor System," *IEEE Trans. Power Del.*, vol. 24, no. 1, pp. 118–123, Jan. 2009.

[5] T. Esmailian, F. R. Kschischang, and P. Glenn Gulak, "In-building power lines as high-speed communication channels: channel characterization and a test channel ensemble," *International Journal of Communication Systems*, vol. 16, pp. 381–400, 2003.

[6] A. M. Tonello and F. Versolatto, "Bottom-Up Statistical PLC Channel Modeling - Part I: Random Topology Model and Efficient Transfer Function Computation," *to appear in IEEE Trans. Power Del.*, 2010.

[7] A. M. Tonello and F. Versolatto, "Bottom-Up Statistical PLC Channel Modeling - Part II: Inferring the Statistics," *IEEE Trans. Power Del.*, vol. 25, no. 4, pp. 2356–2363, Oct. 2010.

[8] D. Schneider, L. Stadelmeier, and D. Schill, "Precoded Spatial Multiplexing MIMO for Inhome Power Line Communications," in *Proc. IEEE Global Commun. Conf. (GLOBECOM)*, Dec. 2008, pp. 1–5.

[9] R. Hashmat, P. Pagani, and T. Chonavel, "MIMO Communications for Inhome PLC Networks: Measurements and Results up to 100 MHz," in *Proc. IEEE Int. Symp. Power Line Commun. and its App. (ISPLC)*, Apr. 2010, pp. 120–124.

[10] J. Anatory, N. Theethayi, and R. Thottappillil, "Power-Line Communication Channel Model for Interconnected Networks - Part II: Multiconductor system," *IEEE Transactions on Power Delivery*, vol. 24, no. 1, pp. 124–128, Jan. 2009.

[11] R. P. Clayton, *Analysis of Multiconductor Transmission Lines*. Wiley-IEEE Press, Nov. 2007.

[12] J. C. Clements, R. P. Clayton, and A. T. Adams, "Computation of the Capacitance Matrix for Systems of Dielectric-Coated Cylindrical Conductors," *IEEE Transactions on Electromagnetic Compatibiliy*, vol. 17, no. 4, pp. 238–248, Nov. 1975.

[13] I. C. Papaleonidopoulos, C. G. Karagiannopoulos, N. J. Theodorou, and C. N. Capsalis, "Theoretical Transmission-Line Study of Symmetrical Indoor Triple-Pole Cables for Single-Phase HF Signalling," *IEEE Trans. Power Del.*, vol. 20, no. 2, pp. 646–654, Apr. 2005.

[14] R. P. Clayton, *Introduction to Electromagnetic Compatibility*, second edition ed. New Jersey: Wiley & Sons, 2006.

[15] J. Dickinson and P. J. Nicholson, "Calculating the High Frequency Transmission Line Parameters of Power Cables," in *Proc. IEEE Int. Symp. Power Line Commun. and its App. (ISPLC)*, Apr. 1997, pp. 127–133.

Fabio Versolatto (SM'10) received the Laurea (Hons.) and the Laurea Specialistica degrees in electrical engineering (Hons.) from the University of Udine, Udine, Italy, in 2007 and 2009, respectively, where he is currently pursuing the Ph.D. degree.

His research interests are power-line communication channel modeling and digital communication algorithms.

Mr. Versolatto received the award for the best student paper presented at IEEE ISPLC 2010.

Andrea M. Tonello (M'00) received the Doctor of Engineering degree in electronics (cum laude), and the Doctor of Research degree in electronics and telecommunications, both from the University of Padova, Italy. On February 1997, he joined as a Member of Technical Staff, Bell Labs - Lucent Technologies, where he worked on the development of baseband algorithms for cellular handsets, first in Holmdel, NJ, and then within the Philips/Lucent Consumer Products Division in Piscataway, NJ. From September 1997 to December 2002, he has been with the Bell Labs Advanced Wireless Technology Laboratory, Whippany, NJ. He was promoted in 2002 to Technical Manager, and was appointed Managing Director of Bell Labs, Italy. In January 2003, he joined the Dipartimento di Ingegneria Elettrica, Gestionale, e Meccanica (DIEGM) of the University of Udine, Italy, where he is an Aggregate Professor.

He received a Lucent Bell Labs Recognition of Excellence award for his work on enhanced receiver techniques in 2003, the award for the best paper published in Eurasip Journal on Advances in Signal Processing about ultra wide band PLC communication 2007, and he is the coauthor of the best student paper award at the IEEE International Symposium on Power Line Communications (ISPLC) 2010. He was co-recipient of two awards in the business plan competition Startcup 2007 and 2008 in Udine, Italy. He was awarded a Distinguished Visiting Fellowship from the Royal Academy of Engineering, UK, in 2010.

He was the TPC Co-chair of IEEE ISPLC 2007, the Chair of the Workshop on Power Line Communications 2009, and the General Chair of IEEE ISPLC 2011. He serves as an Associate Editor for the IEEE Transactions on Vehicular Technology. He is the Vice-chair of the IEEE Communications Society Technical Committee on Power Line Communications.